Journal of Polymer Research (2019) 26: 271
https://doi.org/10.1007/s10965-019-1917-z

ORIGINAL PAPER

Superabsorbent magnetic Fe_3O_4-based starch-poly (acrylic acid) nanocomposite hydrogel for efficient removal of dyes and heavy metal ions from water

Atefeh Saberi[1] · Eskandar Alipour[1] · Mohammad Sadeghi[2]

Received: 17 April 2019 / Accepted: 20 September 2019 / Published online: 16 November 2019

Abstract
Aimed to removal of toxic dyes and heavy metal ions, the magnetic Fe_3O_4-based starch- poly (acrylic acid) nanocomposite hydrogel (Fe_3O_4@St-AcANCH) is designed and synthesized using free radical method. The main procedure for the synthesis of superabsorbent nanocomposite hydrogel is chemical crosslinking of starch and poly (acrylic acid). The as-prepared nanocomposite hydrogel present high removal percentage toward Cu(II), Pb (II), MV and CR solution through a spontaneous physicsorption process that have a good consistence with pseudo-second-order and Langmuir isotherm models. It is indicated that nanocomposite hydrogel is an effective adsorbent for removal of dyes and metal ions which would provide a new platform for water and environmental considerations. Finally, the swelling properties and mechanical parameters of the prepared adsorbents were investigated preliminarily.

Keywords Nano composites · Hydrogels · Starch · Fe_3O_4 nanoparticles · Adsorption

Introduction

The major issues of public interest related to environment are the effective water treatments of chemical contaminations [1]. From toxicity point of view, wide industrial use of heavy metal ions and dyes leads to their perdurable presence in the environment. There are abundant technologies for removing heavy metal and dye from water resources, such as membrane separation, chemical oxidation, coagulation and flocculation, photocatalytic degradation, and adsorption methods [2, 3].

The most common technology of recent years for removal of dyes and heavy metals from wastewaters is adsorption due to the effective procedures, high efficiency, low costs and lack of side effects and toxicity [2, 4, 5]. High-adsorptive and separation performance are two significant properties of an adsorption process [6]. Magnetic separation is a method of wastewater management where magnets are used to separate metal ions from refuse and a promising important process in the beneficiation of environmental purification, thanks to the capability of treating large amounts of wastewater within a short time and no- contaminants productions [7]. By utilizing magnetorheological effects to produce the uniform filler distribution as well as highly anisotropic samples, embedding magnetic nanoparticles in porous materials can improve the absorption capacity [8–10].

Recent developments in biopolymers have an emphasis on natural polysaccharides as treatment agents [11, 12]. Among these, starch [13] chitosan [14] and gum [15] deserve particular attention for application as adsorbents in wastewater treatment because of their biodegradability and non-toxic nature. These materials have proved to be better treatment alternatives compared to their synthetic counterparts because of their particular structure, physicochemical characteristics, chemical stability, high reactivity and excellent selectivity towards heavy metals and dye that cause water pollution.

Starch, a biodegradable agriculturally derived biopolymer, is one of the main neutral polysaccharides specially used in the preparation of green nanocomposites [16] Chemical modification of starch can greatly improve its properties. A variety of starch derivatives containing amide, amino, carboxyl and other groups have been prepared and utilized in water treatment for decades [17].

✉ Mohammad Sadeghi
msadeghi_77@yahoo.com; m-sadeghi@iau-arak.ac.ir

[1] Department of Chemistry, Islamic Azad University, Tehran, North Branch, Iran

[2] Department of chemistry, Islamic Azad University, P.O. Box 38135-567, Arak, Arak branch, Iran

Combining two or more polymers has increasingly become an important technique for the development of new biomaterials with improved properties that could not be achieved by individual polymers [18]. The network structure of hydrogels has attracted considerable attention due to their high water retention, tunable mechanical properties, self-degradation, and environmental applications, which has large application potential in the environment [19–22].

Nanocomposite (NC) gels are considered due to their improved properties, for instance, the extraordinary mechanical property of organic-inorganic hybrid networks of nanocomposite gels [23]. Nano dispersions of metal nanoparticles are used to prepare nanocomposites due to their special properties such as the large surface area to volume ratio and multiple applications. Recently, new composite hydrogels were synthesized based on sulfonic acid-functionalized gum tragacanth (GT) carbohydrate and graphene oxide (GO). Adsorption process for removal of heavy metal ions has the maximum adsorption capacity (q_m) of 142.50, 112.50 and 132.12 mg g^{-1} for Pb(II), Cd(II), and Ag(I), respectively [24]. In the other study, lignin grafted N, N′-methylene-bisacrylamide (LM) was copolymerized with acrylic acid (AA) to fabricate lignin based poly (acrylic acid) (LBPAA) nanocomposites, and organo-montmorillonite (OrgMMT) was uniformly dispersed in LBPAA by ultrasonic method. The Pb^{2+} absorption capacity of LBPAA (PAA 48.50/48.50 LM)/OrgMMT (3 wt%) was reported 1.0803 mmol·g^{-1}, the highest among the composites [25]. Chitosan-crosslinked-poly (alginic acid) nanohydrogel (CN-cl-PL(AA)NHG) was also reported as an effective adsorbent for the exclusion of Cr(VI) metal ion from aqueous medium. It was demonstrated that the prepared chitosan-crosslinked-poly (alginic acid) nanohydrogel had high adsorption tendency for the removal of Cr(VI) from the aqueous solution. The thermodynamic studies showed the adsorption of Cr(VI) onto CN-cl-PL(AA)NHG was spontaneous and chemical in nature [26]. The first incorporation of calcium carbonate nanoparticles (CC NPs) into tragacanth gum (TG) to prepare a new hydrogel nanocomposite (HNC) system using a green, safe, and eco-friendly method, ultrasound irradiation as an efficient biosorbent of heavy metal ions from wastewater was reported by Mallakpour et al. It was found that the Pb^{2+} ions were significantly removed from water using TG/CC HNC 5 wt% and the removal efficiency was determined as 83% at optimized conditions [27]. Peng et al. reported a kind of cellulose–clay hydrogel with superabsorbent properties, superior mechanical performance, and high dye removal efficiency. The as-prepared hydrogels exhibited high absorption capacity for methylene blue (MB) solution through a spontaneous physic-sorption process which fitted well with pseudo-second-order and Langmuir isotherm models. The maximum removal efficiencies of hydrogel samples for MB solutions with concentrations of 10 mg L^{-1} and 100 mg L^{-1} were 96.6% and 98%, respectively [28]. Besides, Hosseinzadeh et al. reported the efficient removal of malachite green (MG) dye from aqueous solution using a novel polysaccharide-based nanocomposite hydrogel adsorbent (NHA). The temperature dependence data also revealed that MG sorption process was feasible, spontaneous and endothermic. Furthermore, the adsorption isotherm data fitted well with the Langmuir isotherm model with a maximum adsorption capacity of 297 mg g^{-1} for MG dye. According to the results, the prepared NHAs could be environment friendly and promising adsorbents for the adsorption of different cationic dyes from contaminated water [29]. The magnetic nanocomposite hydrogel (m-CVP) beads were also prepared by instantaneous gelation of carboxymethyl starch-*g*-polyvinyl imidazole (CMS-*g*-PVI), poly (vinyl alcohol) (PVA), and Fe_3O_4 mixture in boric acid solution followed by crosslinking by glutaraldehyde (GA). Highly porous m-CVP beads with magnetic sensitivity were fully characterized and used as eco-friendly adsorbent for the removal of crystal violet (CV) and congo red (CR) dye and Pb(II), Cu(II) and Cd(II) from water. Batch adsorption results showed that the sorbent had high affinity to the heavy metals and dyes in water. All the studied results indicated that m-CVP beads were an efficient, low cost, and reusable adsorbent for the removal of dye and heavy metal ions from aqueous solutions [30].

In the present study, Acrylic acid was radically copolymerized onto macromolecular chains of starch in the presence of ammonium persulfate as an initiator to afford a water soluble St-AcAH copolymer. Then, a mixture of St-AcAH and Fe_3O_4 nanoparticles was used in the preparation of magnetic hydrogel nanocomposite (Fe_3O_4@St-AcANCH) crosslinking by N, N-methylene bis acrylamide. The prepared magnetic hydrogel nanocomposite was characterized by FT-IR, scanning electron microscopy (SEM), vibrating sample magnetometer (VSM), X-ray diffraction (XRD), energy-dispersive X-ray spectroscopy (EDX), transmission electron microscopy (TEM) and thermal gravimetric analysis (TGA). The adsorption equilibrium of a cationic dye, methylene violet (MV), and an anionic azo dye, congo red (CR), and heavy metal ions, i.e. Cu(II), and Pb(II) Cd(II) from aqueous solutions on Fe3O4@St-AcANCH was investigated in detail. The effects of various parameters such as initial dye and heavy metal ion concentration, contact time, and temperature on adsorption were studied to investigate adsorption isotherms, kinetics and thermodynamics. Adsorption-desorption experiments were also undertaken to find out the reusability of the adsorbent.

Materials and methods

Materials

Soluble starch (Mw = 342.30), Congo Red (CR) and Methylene Violet (MV) dye were purchased from Sigma-Aldrich. Acrylic acid (AcA; MW =72.06 g mol^{-1}, d =

1.06 g/cm^3) and ammonium persulfate (APS) were purchased from Fluka and used after vacuum distillation. N, N-methylene bis acrylamide (MBA) and lead(II) nitrate and copper(II) sulfate were purchased from Merck and used as received.

Synthesis of starch-based/AcA hydrogel (St-AcAH)

Briefly, a definite amount of starch was solved in warm water at 80 °C. After 15 min, a certain amount of MBA was dissolved in water (5 mL) and added to the aqueous solution with continuous mechanical stirring (300 rpm) until a homogeneous viscous mixture was obtained. The reaction temperature was controlled at 50 °C under an argon atmosphere, then a certain amount of 70% neutralized AcA was added to the reaction mixture. At the next step, a definite amount of APS solution was added into the mixture and was stirred for 10 min until the hydrogel was produced. After cooling to room temperature, the reaction was neutralized with a certain amount of alkaline solution. Afterward, the reaction mixture was left over night in ethanol (100 mL). In the last step, the hydrogel was filtered and dried at 50 °C.

Preparation of Fe_3O_4 nanoparticles

Magnetic Fe_3O_4 nanoparticles were prepared by conventional co-precipitation method. $FeCl_3.6H_2O$ (10 mmol, 2.730 g) and $FeCl_2.7H_2O$ (5 mmol, 0.994 g) were dissolved in deionized water (20 mL) and stirred at 80 °C. Then, 80 mL NH_4OH solution (1.5 M) was added into the mixture under N_2 atmosphere until the pH reached 10 and the reaction mixture was stirred for 1 h. The formed black precipitate was separated by an external magnet, and then was washed several times with deionized water.

Synthesis of Fe_3O_4-starch/AcAnanocomposite hydrogel (Fe_3O_4@St-AcANCH)

For the synthesis of Fe_3O_4@St-AcANCH, the procedure of section 2.2 was repeated; but after adding APS, the as-prepared Fe_3O_4 colloidal solutions were mixed with the above homogeneous solution and allowed to stir for 10 min. When the reaction was completed, the product was washed thoroughly with ethanol (100 mL) to remove the unreacted materials. The Fe_3O_4@St-AcANCH hydrogel nanocomposite with weight ratios (*w*/w) of (St-AcANCH): (magnetite) 2: 1 was prepared by chemical crosslinking by MBA. It is worth noting that the magnetic hydrogel nanocomposite was recovered with the help of an external magnet in order to remove unreacted chemicals. Finally, the final product was rinsed with distilled water and dried at 50 °C in a vacuum oven.

Characterizations

The morphology characteristics of synthesized samples were evaluated using scanning electron microscopy (SEM, Hitachi S-4800). The thermo gravimetric analysis (TGA) was measured under a nitrogen atmosphere with a TG/DTA7300 from room temperature to 700 °C with the heating rate of 10 °C/min. The functional groups of samples were detected using FT-IR American Nicolet 5700 spectrophotometer. The crystal phases of the samples were analyzed using X-ray diffractometer (XRD, M21X, MAC Science Ltd., Japan) with Cu-Kα radiation. UV-vis diffuse reflectance spectra (DRS) were recorded on a UV-vis spectrophotometer (Cary 300, USA) with an integrating sphere. The chemistry of the surface of bioadsorbentswas also determined using X-ray photoelectron spectroscopy (XPS, K-Alpha 1063, Thermo Fisher Scientific, and England). A vibrating sample magnetometer (VSM) (Kavir Magnetic Co. Iran) was used to evaluate the room temperature magnetic parameter of Fe_3O_4 and magnetic hydrogel nanocomposite with an applied field from −10,000 to +10,000 Oe.

Adsorption measurements

Batch experiments were conducted to study the adsorption behavior of methylene violet (MV, a cationic dye), congo red (CR, an anionic azo dye) and Pb(II), and Cu(II), heavy metal ions, onto Fe_3O_4@St-AcANCH in aqueous media. For determination of the optimum dosage of the adsorbent, the adsorption experiments were carried out using Fe_3O_4@St-AcANCH (0.01–0.5 g) in the solution of dyes (150 ppm) and heavy metal ions (100 ppm), and the mixture was stirred at 600 rpm at 25 °C for 5 h. The effect of pH was studied in the range 2–8 for heavy metal ions and dyes. The pH of the initial solution was adjusted to the required pH value using either 0.1 M HNO_3 or 0.1 M NaOH. The concentration of heavy metal ions was determined with an atomic absorption spectrophotometer (nov AA 400p, Germany). The removal percentage (Removal, %) and the adsorption capacity (qe, mg g^{-1}) of the hydrogel was calculated using the following equations:

$$q_e = \frac{(C_0 - C_e)}{m} \times V \quad (1)$$

$$Removal = \frac{(C_0 - C_e)}{C_0} \times 100 \quad (2)$$

where the amount of dye and heavy metal ions (mg g^{-1}) adsorbed at equilibrium is defined by q_e. C_o and C_e are the initial and equilibrium concentrations of adsorbent materials (mg L^{-1}), respectively. The mass of hydrogel (g) and the volume of the metal ion solution (L) are specified respectively by m and V.

Desorption measurements

Desorption of MV dye is carried out in 200 mL ethanol for 10 h at room temperature while desorption of CR is performed in 0.1 M NaOH solution (100 mL). Desorption of heavy metal ions is carried out in 0.01 M HNO_3 solution (100 mL). After removing hydrogel from desorption solution using an external magnet, the hydrogel is washed with distilled water, dried at 60 °C, and used for the subsequent runs. The eluted MV, CR, Pb(II) and Cu(II) were measured according to Eq. (3). In this equation, C_d is the metal ions concentration in the desorption solutions (mg L^{-1}) and V_d is the volume of the desorption solution in a liter, respectively and V is the volume of the solution in a liter. The adsorption-desorption cycles were repeated seven times using the same adsorbents.

$$\%D = \frac{C_d V_d}{(C_0 - C_e)\, V} \times 100 \quad (3)$$

Result and discussion

Polymerization procedure of St-AcAH and Fe_3O_4@St-AcANCH

Free radical polymerization involved for stabilization of nanoparticles [31] has been used for the preparation of both bioadsorbents. Random free radical polymerization of AcA onto starch by sequential crosslinking method accomplished according to Table 1. The optimum procedure for the polymerization of St-AcAH and Fe_3O_4-St-AcANCH is observed for 70% neutralization.

Heating leads to the decomposition of APS (0.03 mol L^{-1}) as the thermal initiator and preparation of sulfate anion radical. Abstraction of hydrogen from one of the existing hydroxyl groups in starch backbone (4w/w) is occurred to form the corresponding macro-initiator on the substrate. The redox pair systems, i.e. (starch-APS) lead to copolymers initiated by radically active centers capable of initiated polymerization of AcA monomers (1.2 mol L^{-1}). Subsequently, the presence of crosslinker (MBA, 0.006 molL^{-1}) or co-crosslinker agent (Fe_3O_4, 0.02 g) in the reaction mixture prepared a crosslinked structure as shown in Scheme 1.

Characterization of St-AcAH and Fe_3O_4@St-AcANCH adsorbents

FTIR spectroscopy

FTIR spectroscopy was employed to confirm the chemical structure of prepared bioadsorbents. Figure 1 showed the FTIR spectra of prepared St-AcAH and Fe_3O_4@St-AcANCH samples. The broad band at 3000–3600 cm^{-1} was related to the stretching vibration of OH groups on both starch biopolymers. The skeletal mode vibration of the glycoside linkage is illustrated at 900–950 cm^{-1}. In the spectrum of St-AcAH bioadsorbent, the characteristic absorption peaks at 1646 and 1796 cm^{-1} were assigned to stretching of carboxamide and carbonyl groups in crosslinker and acrylic acid monomers, respectively. The peak around 2950 cm^{-1} and 1460 cm^{-1} are related to the CH stretching and bending mode. Meanwhile, two other characteristics peaks of carboxylate ion were clearly visible for St-AcAH [32]. The first peak is at about 1413 cm^{-1}, assigned to the symmetric stretching mode of the carboxylate ion, while the second peak is at the range of 1540–1510 cm^{-1} due to the asymmetric stretching mode of COO^- groups [33]. These results suggested that the grafted acrylic acid monomers were a presence in two forms of non-ionized (COOH) and ionized (COO^-) onto the polymer backbone [34].

On the other hand, the FTIR spectrum of the nanocomposite hydrogel showed several new peaks (Fig. 1). The data indicated the inclusion of Fe_3O_4 in the polymer matrix effect on the position of functional groups present Fe_3O_4@St-AcANCH. In fact, the shifts in basic peaks position from 3425 cm^{-1} to 3410 cm^{-1} related to NH or OH groups, and 1796 cm^{-1} to 1740 cm^{-1} related to carboxylate groups were corresponding to the formation of an interpenetrating network between O and N atoms of carboxylate and $–NH_2$ groups of

Table 1 Optimum contents and conditions in the synthesis of St-AcAH and Fe_3O_4@St-AcANCH

	Starch(w/w)	APS (mol L^{-1})	AcA (mol L^{-1})	Fe_3O_4 (g)	MBA (mol L^{-1})	Neutralization
St -AcAH	1	0.03	0.1	0	0.01	30%
	2	0.03	0.5	0	0.009	40%
	3	0.03	1.0	0	0.007	60%
	4	**0.03**	**1.2**	**0**	**0.006**	**70%**
Fe_3O_4@St-AcANCH	4	0.03	1.2	0.5	0.006	50%
	4	0.03	1.2	0.2	0.006	60%
	4	0.03	1.2	0.1	0.006	65%
	4	0.03	1.2	0.05	0.006	68%
	4	**0.03**	**1.2**	**0.02**	**0.006**	**70%**

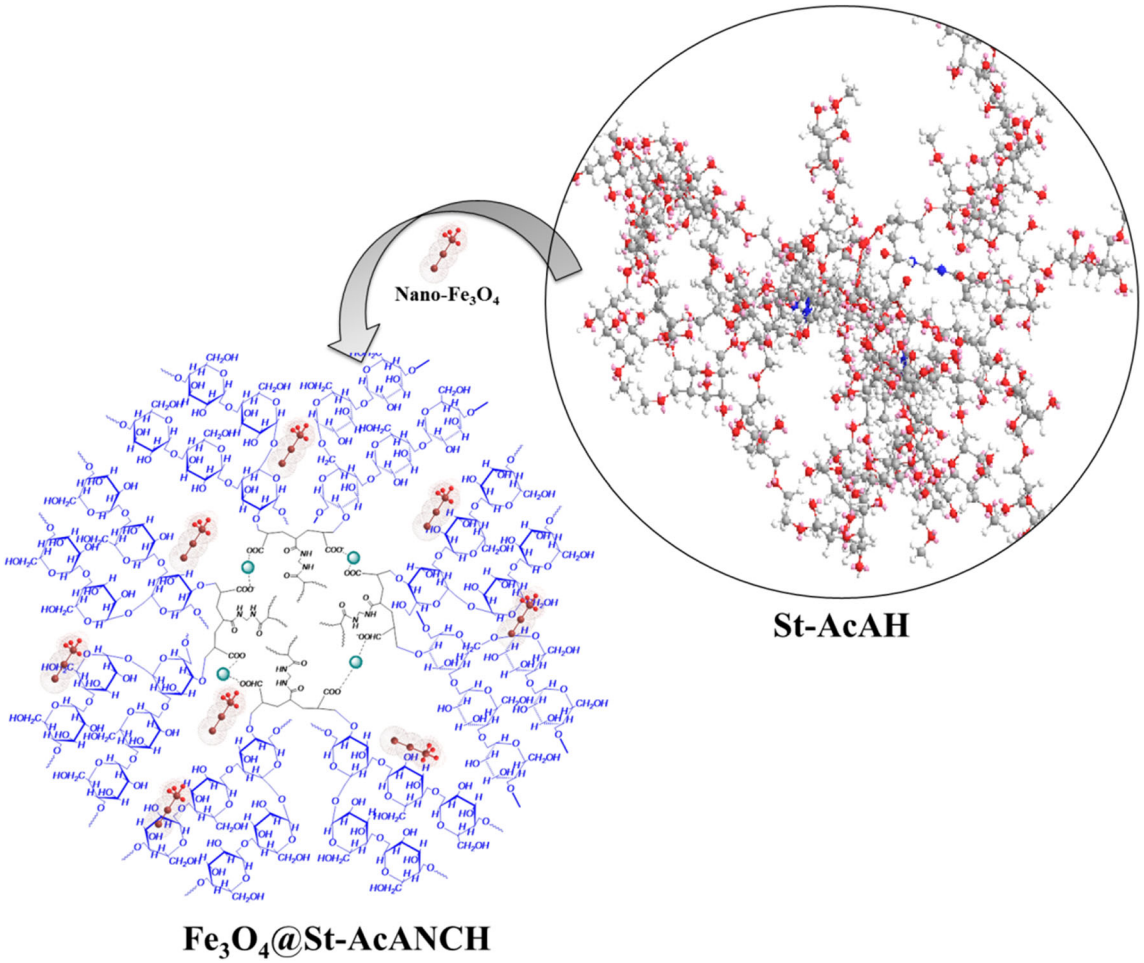

Scheme 1 Free radical polymerization of Fe_3O_4@St-AcANCH

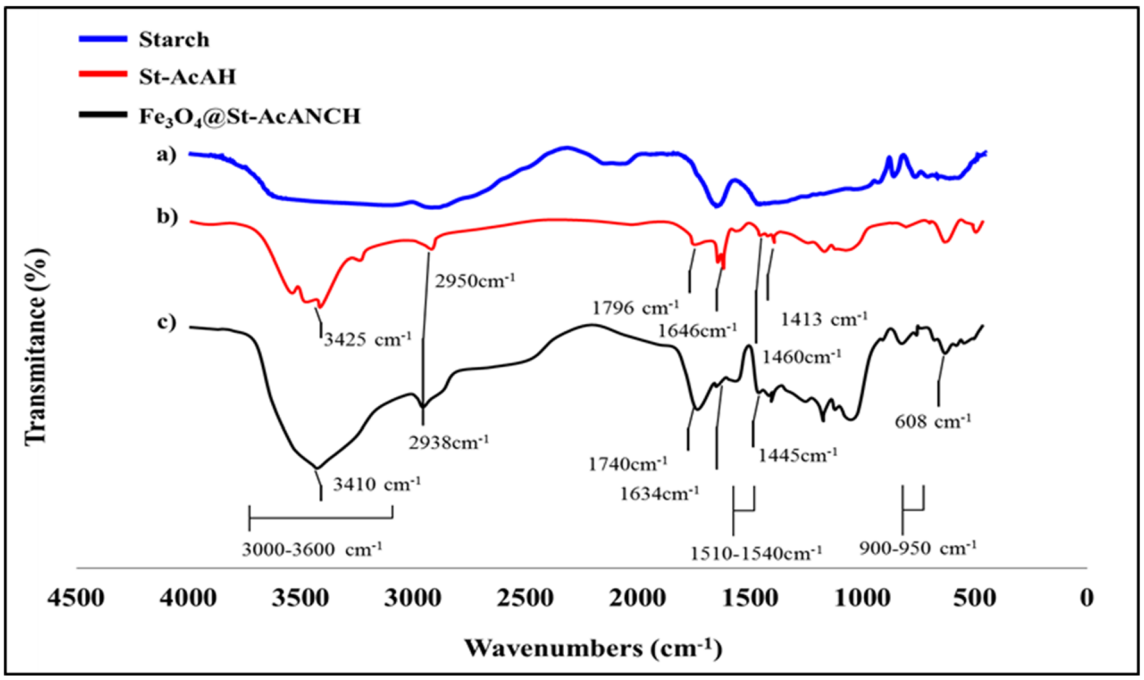

Fig. 1 IR spectrum of starch, St-AcAH, Fe_3O_4@St-AcANCH

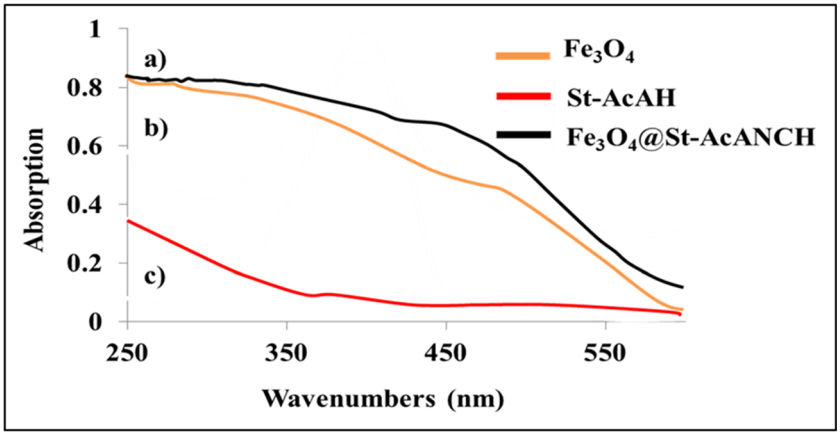

Fig. 2 UV-visible spectrum of Fe_3O_4 nanoparticles, St-AcANCH, and Fe_3O_4@St-AcANCH

Fe_3O_4@St-AcANCH with Fe_3O_4, which leaded to broadening and shifting the functional groups. The presence of $Fe_3O_4$is illustrated due to the peak at 608 cm^{-1} which is related to the Fe-O bond in of Fe_3O_4 nanoparticles. Therefore, these finding preliminarily indicated that the Fe_3O_4-St-AcANCH had been synthesized.

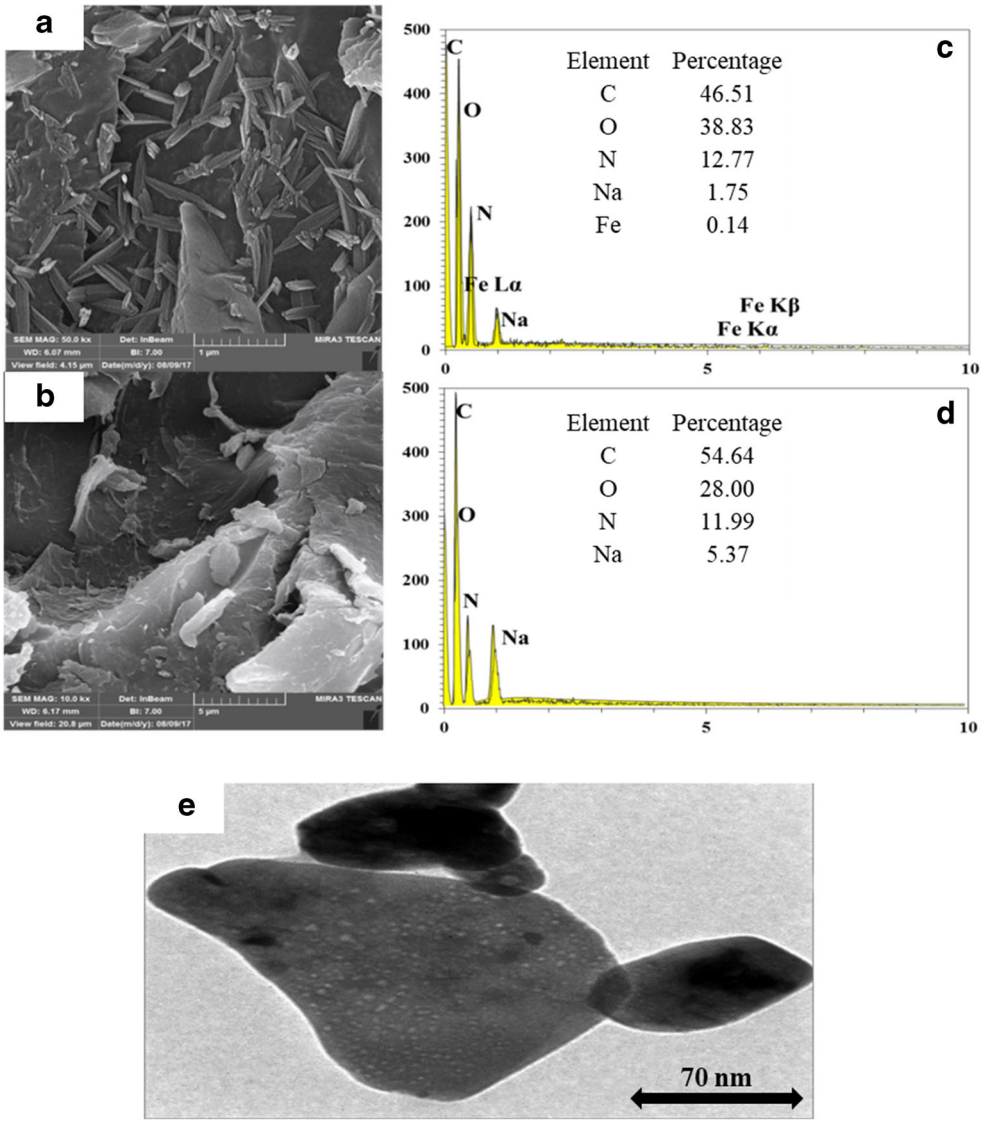

Fig. 3 SEM, EDX of Fe_3O_4@St-AcANCH (A and C) St-AcAH (B and D), and TEM image for Fe_3O_4@St-AcANCH (E)

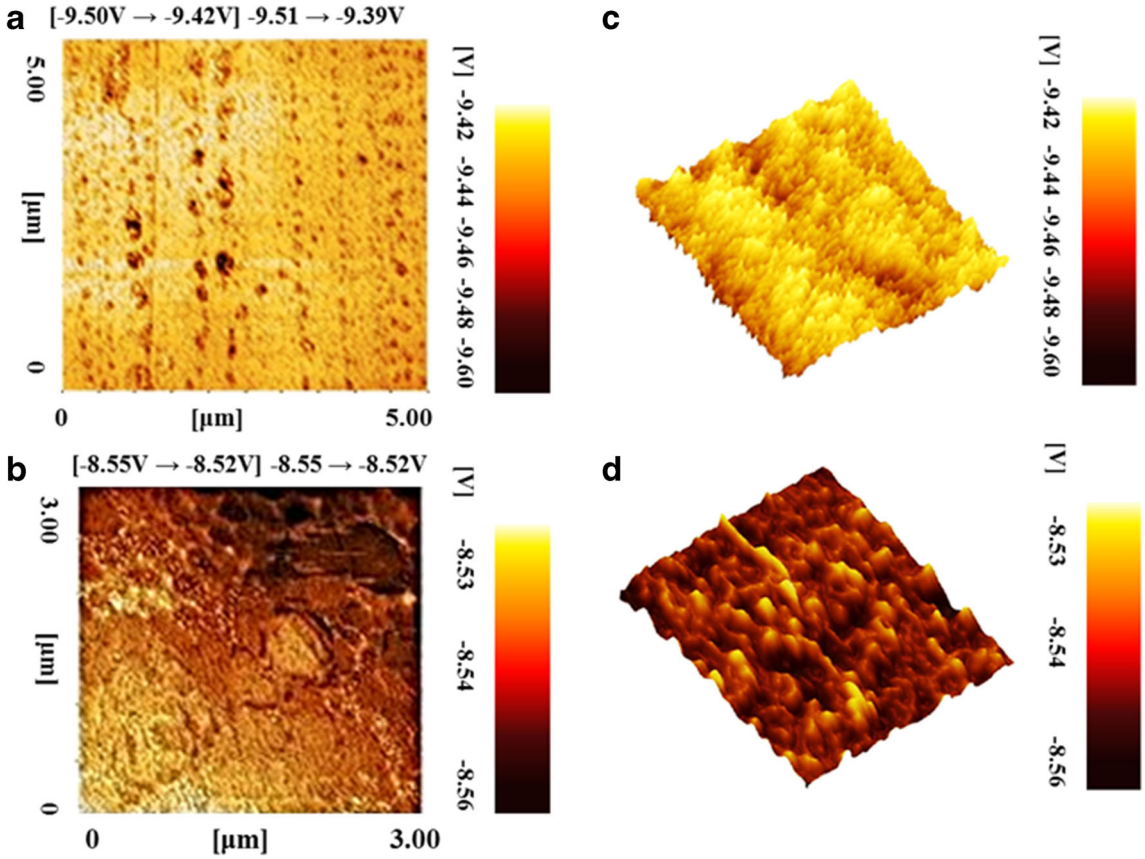

Fig. 4 AFM images for St-AcAH (A, C), Fe_3O_4@St-AcANCH (B, D)

UV-vis spectroscopy

Figure 2 Shows UV-vis spectroscopy spectra of Fe_3O_4@St-AcANCH compared with St-AcAH and Fe_3O_4 nanoparticles.

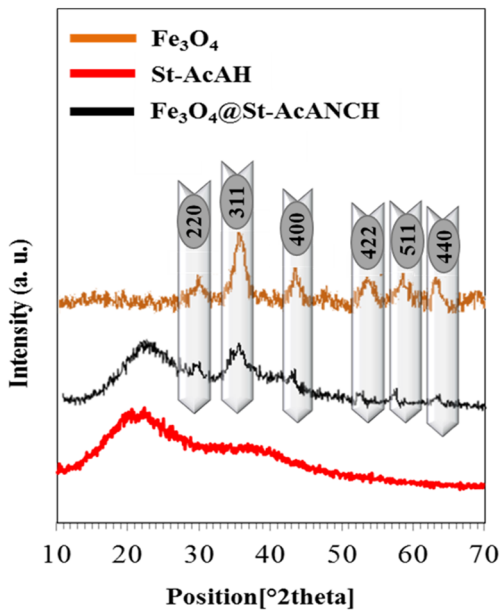

Fig. 5 XRD patterns of Fe_3O_4 nanoparticles compared with St-AcAH and Fe_3O_4@St-AcANCH

As can be seen in Fig. 2, St-AcAH did not absorb in UV-vis spectrum, although Fe_3O_4 nanoparticles appeared a single broad peak with a maximum wavelength at about 200–400 nm, which is attributed to the d-orbital transitions of Fe_3O_4 [35]. In case of Fe_3O_4@St-AcANCH, the intensity of absorption pattern was increased, but there was no specific absorption band was appeared due to the mixed transition of composite. Based on the above results and the presence of Fe_3O_4 nanoparticles in the nanocomposite hydrogel matrix, it is concluded that very stable nanoparticles of Fe_3O_4 were formed and dispersed in the Fe_3O_4@St-AcANCH matrix while no conjugated bond is formed

SEM, EDX, TEM and AFM analyses

SEM, TEM, EDX, and AFM techniques have been used to evaluate the incorporation of Fe_3O_4 nanoparticles into the Fe_3O_4@St-AcANCH matrix, the morphology and topography both of bioadsorbents. In **Fig. 3A** and **B**, it was clearly indicated that both of bioadsorbents had porosity structures, while the surface morphology Fe_3O_4@St-AcANCH shows a cluster porosity which is rougher than St-AcAH. Figure 3C and D showed the elemental composition of bioadsorbents, it was calculated that Fe_3O_4@St-AcANCH contained about 46.51% of carbon, 38.83% of oxygen, 12.77% of nitrogen, 1.75% of sodium, and 0.14% of iron. The results confirmed the deposition of Fe_3O_4

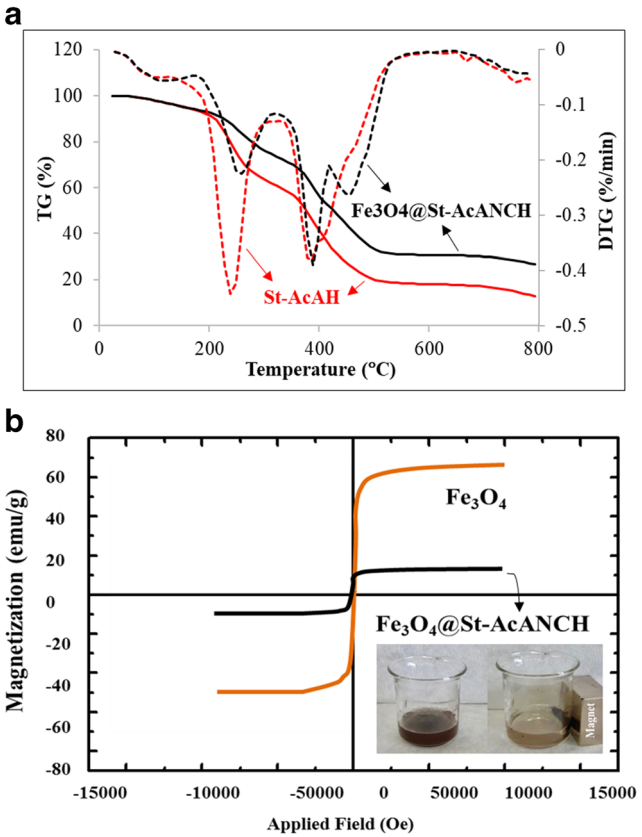

Fig. 6 TGA and DTG of St-AcAH, Fe_3O_4@St-AcANCH (A) and VSM image of Fe_3O_4@St-AcANCH compared with Fe_3O_4 and using magnet for separation of nanocomposite (B)

nanoparticles in the nanocomposite hydrogel matrix. The morphology, shape, and distribution of Fe_3O_4 size were determined by analyzing the TEM images of the nanocomposite hydrogel. The image of TEM was shown in Fig. 3E and confirmed a highly uniform distribution of the spherical Fe_3O_4 with the size particles 70 nm inside the nanocomposite hydrogel.

In Fig. 4, AFM images were depicted the surface morphology of the bioadsorbents. Comparing the 2D and 3D images in Fig. 4 **A-D**, the surface morphology for St-AcAH was shown to be a smooth while for Fe_3O_4@St-AcANCH nanocomposite was a rough surface with clustered features.

XRD analysis St-AcAH and Fe_3O_4@St-AcANCH adsorbents

Analyzing the structure of both bioadsorbents using X-ray diffraction was illustrated in Fig. 5. As shown in the XRD patterns, St-AcAH had no characteristics peaks, which confirmed its amorphous nature. In contrast, Fe_3O_4@St-AcANCH exhibited relative sharp peaks at $2\theta = 30.1°$, 35.4°, 44.34°, 55.0°, 57.3° and 63.2° which were assigned to the planes of crystal structure of Fe_3O_4 nanoparticles. In addition, the slight reduction of XRD patterns of the nanocomposite and Fe_3O_4 can be related to the coating of Fe_3O_4 nanoparticles on the nanocomposite matrix [36, 37].

TGA/DTG analysis

Figure 6A represented the TGA/DTG analysis of both prepared bioadsorbents. Two steps of decomposition were seen for St-AcAH. The first weight loss at 150–250 °C was due to loss of moisture present in the dry hydrogel and the second rapid weight loss was due to the thermal degradation of the organic content of St-AcAH structure in the range 350–450 °C. Similar decomposition steps at the same temperature were also seen for Fe_3O_4@St-AcANCH compared to St-AcAH hydrogel. According to Fig. 6A, the resulted weight loss for the nanocomposite at 277 °C (18.2%) and 500 °C (69.3%) are lower compared to that of the St-AcAH hydrogel (54.1% and 79.8%), respectively [38]. However, this can be attributed to the high thermal stability of the Fe_3O_4 nanoparticles and to the interaction between these nanoparticles and the polymer matrix.

VSM analysis

The magnetic properties of iron oxide nanoparticles and nanocomposite have been investigated by VSM, as shown in Fig. 6B. It is very important to note that absorbents of this kind should have sufficient and supermagnetic properties. The saturation magnetization coefficient (σ_s) of nanocomposite is about 22.14 emu g^{-1}, which is much lower than the iron oxide nanoparticle. The reason for this decrease in the magnetic property is the covering of iron oxide nanoparticles with hydrogel chains. However, the magnetic strength of magnetic nanocomposite is sufficient to separate in a soluble phase by an external magnet that is observed in figure.

Swelling properties and mechanical characterization

Swelling capacity is believed to be a one of the most important properties of adsorbents to effect final efficiency on removal of

Table 2 Swelling properties and mechanical parameters of the prepared St-AcAH and Fe_3O_4@St-AcANCH adsorbents

Samples	Swelling (g/g)	Hardness (MPa)	Young's modulus (MPa)
St -AcAH	120.8	5.1	2.5
Fe_3O_4 (0.1)@St-AcANCH	147.4	6.7	3.1
Fe_3O_4 (0.2)@St-AcANCH	166.3	7.2	3.4
Fe_3O_4 (0.5)@St-AcANCH	152.7	7.8	3.7

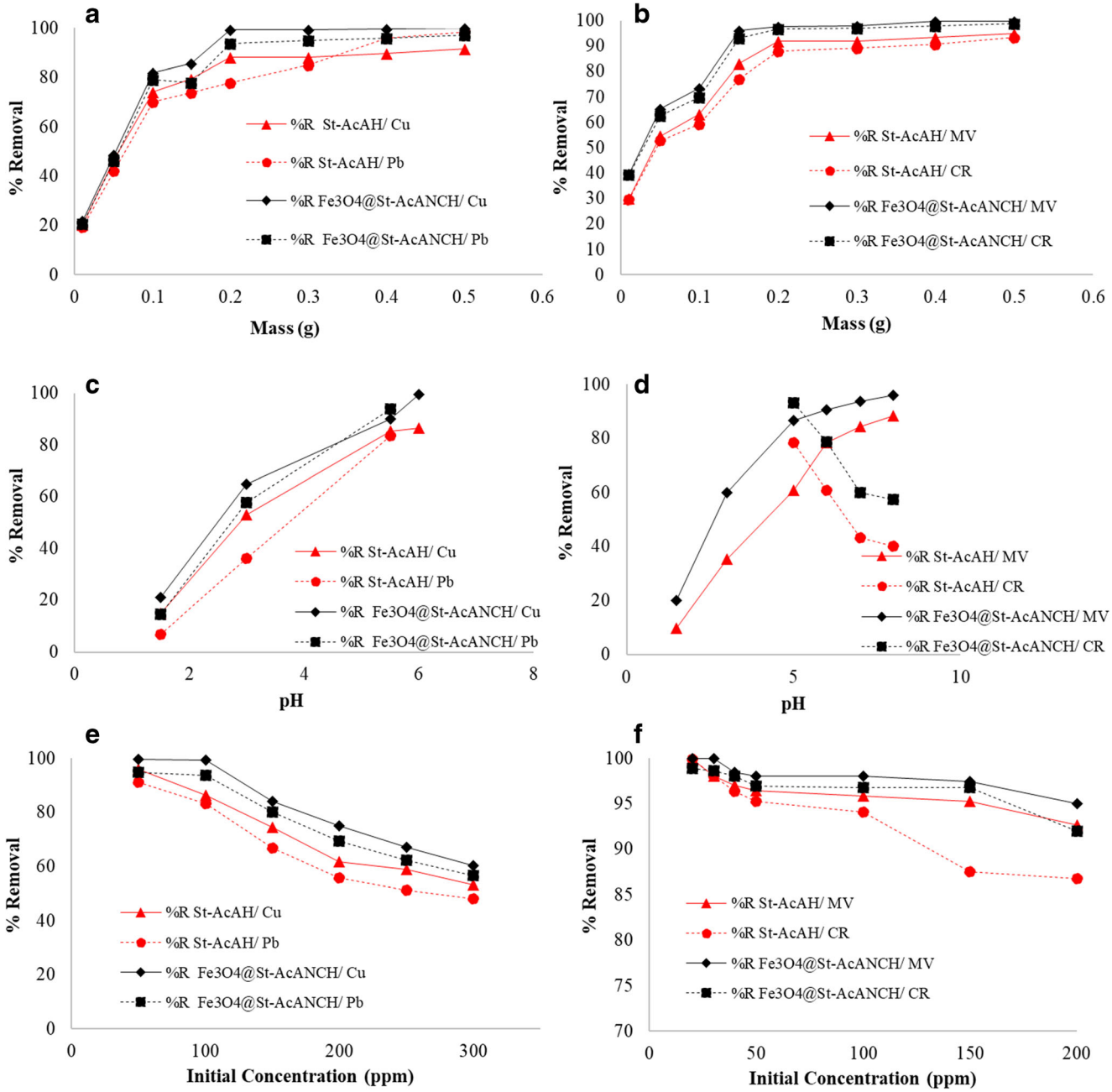

Fig. 7 Effects of bioadsorbent mass (A and B), pH solution (C and D) and the initial concentration (E and F) on removal of metal ions and dyes removal percentage

heavy metal ions. To this purpose, the swelling behavior of the prepared adsorbents was investigated and the result is listed in Table 2**.** According to the table, obtained results showed that swelling amount of the Fe_3O_4@St-AcANCH nanocomposites was more than St-AcANCH hydrogel and the swelling amount of nanocomposites was also increased with increasing in Fe_2O_3 NPs content. The highest swelling capacity was found for Fe_3O_4@St-AcANCH with 0.2 g Fe_2O_3 NPs content. This high capacity can be attributed to further crosslinking of polymeric chains to form highly interconnected that led to more diffusion of water molecular into the micropores of polymer matrix. A similar result has been reported by Dong-Wan Cho et al. [39]. On the other hand, effect of Fe_2O_3 NPs content onto mechanical properties of the prepared nanocomposites was investigated. The results showed that nanocomposites in compared to hydrogels possessed a highly mechanical strength, so that the optimum nanocomposites exhibited hardness and young's modulus at 7.2 MPa and 3.4 MPa, whereas that for hydrogel was 5.1 MPa and 2.5 MPa, respectively [40]. As can be seen in Table 2, with increasing amount of Fe_2O_3 NPs from 0.1 g to 0.5 g, the hardness and young's modulus of the nanocomposite enhanced significantly from 6.7 and 3.1 MPa to 7.8 and 3.7 MPa, respectively.

Table 3 Thermodynamic parameters of bioadsorbents for removal of pollutants

Pollutants		Thermodynamic parameters							
		lnK_c			ΔG (kJ/mol)			ΔH (K/mol)	ΔS (J/Kmol)
		298 K	308 K	318 K	298 K	308 K	318 K		
Cu(II)	St-AcAH	1.854	2.410	4.022	−4.597	−6.174	−10.638	84.977	298.921
	Fe_3O_4@St-AcANCH	4.984	8.516	10.819	−12.354	−21.820	−28.619	230.555	816.127
Pb(II)	St-AcAH	1.609	2.015	2.721	−3.988	−5.163	−7.199	43.728	159.595
	Fe_3O_4@St-AcANCH	2.716	3.346	3.891	−6.734	−8.574	−10.294	46.360	178.144
MV	St-AcAH	3.007	5.132	10.819	−7.456	−13.149	−28.619	306.404	1047.564
	Fe_3O_4@St-AcANCH	3.649	4.304	11.225	−9.047	−11.026	−29.691	295.928	1014.142
CR	St-AcAH	1.950	3.199	3.912	−4.835	−8.195	−10.348	77.552	276.964
	Fe_3O_4@St-AcANCH	3.409	4.304	5.003	−8.451	−11.026	−13.235	62.932	239.617

Metal ions and dyes removal evaluation

Evaluation of the rate and adsorption capacity of metal ions (Cu(II) and Pb(II)) and dyes (MV and CR) aqueous solution is performed using the various kinetic and thermodynamic analyses such as the effect of bioadsorbent mass, the initial metal ions and dyes concentrations, effect of temperature and thermodynamics and other important factors.

Effect of bioadsorbent mass and pH solution

Reaching the maximum metal ions and dyes removals, determining the optimal bioadsorbent mass loaded would be one of the important steps. Therefore, the range of 0.01–0.5 g was examined at 298 K and metal ions concentration of 100 ppm or dyes concentration of 150 ppm to find the effects of amount bioadsorbents for removal of Pb(II), Cu(II), MV and CR (Fig. 7 **A and B**). It is observed that the increasing of the amount of bioadsorbents resulted in an increase of Pb(II) and Cu(II) percentage removal, with a maximum of 93.83% and 99.32% and CR and MV dyes with maximum adsorption of 96.7% and 97.5% for Fe_3O_4-St-AcANCH (0.2 g) respectively. In fact, at optimum condition can be said that the possibility of formation of complexes between the studied bivalent metal ions or dye and functional groups onto adsorbents was increased. However, the adsorption capacity of bioadsorbent was decreased at higher concentrations. It could be concluded that at the lower level of bioadsorbent content in the reaction mixture, there were more available active sites for trapping the metal ions and dyes, so the adsorption capacity is increased. At higher levels, the system reached equilibrium at lower concentrations of adsorbed metal ions and dyes indicating that the number of unsaturated active sites onto bioadsorbent decreased [41].

The pH value of the medium is also an important factor in the adsorption process as it influences the surface properties of the adsorbent and ionization/dissociation of the chelating groups. Figure 7C and D shows the effect of pH on absorbing the metal ions and dyes. It has been shown that the adsorption of Cu (II) and Pb (II) metal ions strongly depends on pH because it affects the solubility and ionization state of functional groups such as hydroxyl groups on the adsorbent.

To investigate the influence of solution pH on the removal efficiency, sorption experiments were carried out at a pH range of 2–6 for heavy metal ions. At pH > 6, the precipitation of heavy metal ions occurred simultaneously, this could lead to the error of adsorption data. The solution pH was in the range of 2–8 for MV and 5–8 for CR. The

Table 4 Kinetic parameters for St-AcAH and Fe_3O_4@St-AcANCH adsorbents

Adsorbent	Pollutants	pseudo-first-order			pseudo-second-order		
		q_e	K_1	R^2	q_e	K_2	R^2
St-AcAH	Cu(II)	28.465	0.010	0.817	29.4	1.85E-05	0.966
Fe_3O_4@St-AcANCH		48.962	0.015	0.798	50.66	8.76E-05	0.989
St-AcAH	Pb(II)	27.851	0.015	0.681	29.33	1.63E-06	0.961
Fe_3O_4@St-AcANCH		46.465	0.019	0.731	48.9	7.52E-05	0.987
St-AcAH	MV	47.696	0.015	0.767	49.6	2.77E-05	0.988
Fe_3O_4@St-AcANCH		72.755	0.021	0.805	74.1	2.1E-05	0.982
St-AcAH	CR	43.933	0.016	0.808	45.65	5.09E-05	0.985
Fe_3O_4@St-AcANCH		71.825	0.017	0.844	73.6	1.74E-05	0.989

adsorption of MV was measured in the pH region of 2–8 because the color of the solution and the maximum wavelength of MV did not change in this region. However, it is notable that under highly acidic pH < 2, protonation of the functional groups onto sorbents and dye leads to a decrease in the electrostatic attractions between the surface of the sorbents and the dyes which that are responsible for the high filter efficiency and adsorption of dyes [42]. However, there are various chelating groups in the magnetic nanocomposite such as carboxylic acid (-COOH) and hydroxyl (-OH) which can accept or donate protons at different pH values. The removal efficiency for the metal ions and dyes (cationic and anionic) depends on the nature of charges of the magnetic nanocomposite. According to the results shown in Fig. 7C and D, the removal efficiency of metal ions and cationic dye (MV) increased with increasing the initial pH value of the solution. This was due to the deprotonation of sulfonic and carboxylic acid groups at the basic solution, and the specific interactions between the adsorbates and adsorbent. These strong interactions can be created through dipole–dipole interactions of highly polarized surface related to adsorbents [43]. On the other hand, the active groups of magnetic nanocomposite were protonated in acidic solution and competition between proton and cationic dyes or metal ions for adsorption sites led to the decrease of the removal efficiency [44].

The highest removal efficiency for Cu(II) (95.4%), Pb(II) (88.4%), and MV (93.66%) is shown at pH 6.0, 5.5 and 7.4, respectively. On the other hand, the removal of anionic dye (CR) increased with decreasing pH from 8 to 5 and the best result is observed at pH = 5. It should be noted that CR is insoluble in water and its color change occurred at pH <5. This is due to the protonation of the active groups in the acidic solution. The positively charged active groups attracted the sulfonate ion groups of CR molecules leading to the increase of the removal efficiency. With increasing pH, deprotonation occurred with the formation of negative nanocomposite and led to the decrease in CR adsorption [44]. It is showed the highest removal efficiency (93.1%) for CR at pH 5.

Effect of heavy metal ions and dye concentrations

The effect of the initial concentration of heavy metal ions in the range of 50–300 ppm is investigated at 298 K for Fe_3O_4@St-AcANCH (0.2 g) and St-AcAH (0.3 g). As shown in Fig. 7E, an increase in the initial concentration of heavy metal ions in the range of 50–300 ppm resulted in a decrease in the percentage of the removal ability of both biodegradable. The higher concentration of heavy metal ions results in constant adsorption of Cu (II) and Pb (II), which means the occupation or saturation of active sites of adsorbents. The optimum adsorption capacity for the Fe_3O_4@St-AcANCH hydrogel magnetic nanocomposite was 100 ppm for Cu (II) and Pb (II) ions. The effect of initial concentration of CR and MV dyes is investigated in the range of 20–200 ppm at 298 K for Fe_3O_4@St-AcANCH (0.2 g) and St-AcAH (0.3 g). As shown in Fig. 7F, the increase of dyes concentration has also a negative effect. The optimum adsorption capacity of the absorption capacity is considered at 150 ppm for CR and MV for Fe_3O_4@St-AcANCH hydrogel magnetic nanocomposites.

Investigating thermodynamic parameters

The effect of temperature on heavy metal ions and dyes removal was carried out at three different temperatures 298 K, 308 K, and 318 K. As shown in Table 3, the thermodynamic parameters such as Gibb's free energy change (ΔG°, kJ/mol), enthalpy change (ΔH°, kJ/mol), and entropy changes (ΔS°, J/K mol) were estimated according to Eq. 4 and 5:

$$\Delta G = -RTlnb \tag{4}$$

$$lnK_c = \frac{-\Delta H^*}{RT} + \frac{\Delta S^*}{R} \tag{5}$$

where, R is the gas constant (8.314 J/mol K), K_c (q_e/C_e) is adsorption affinity, and T is the temperature (K). The enthalpy change (ΔH°) and entropy change (ΔS°) were also calculated from the slope and intercepted of $\ln K_c$ versus 1/T, respectively.

Table 5 Summary of isotherm parameters for the adsorption of heavy metal ions and dyes on St-AcAH and Fe_3O_4@St-PEG-AcANCH

Adsorbents	Pollutants	Langmuir			Freundlich		
		q_{max}	b	R^2	n	K_F	R^2
St-AcAH	Cu(II)	44.64286	0.183	0.9976	3.732	13.867	0.9856
Fe_3O_4@St-AcANCH		74.62687	0.827	0.9918	6.131	10.811	0.8194
St-AcAH	Pb(II)	40.81633	0.127	0.9983	3.405	39.939	0.9417
Fe_3O_4@St-AcANCH		74.07407	0.194	0.9967	3.262	21.071	0.8624
St-AcAH	MV	17.094	4.534	0.9402	5.120	12.953	0.9041
Fe_3O_4@St-AcANCH		23.584	47.111	0.9814	10.070	22.615	0.7849
St-AcAH	CR	16.778	4.226	0.9632	5.431	12.468	0.9327
Fe_3O_4@St-AcANCH		31.847	2.065	0.999	2.188	20.897	0.9705

The negative amounts of ΔG° for both bioadsorbents were seen at all investigated temperatures (Table 3). In addition, increasing the temperature from 298 to 318 K showed more effective sorption of heavy metal ions and dyes on both of bioadsorbents at the highest temperature. On the other hand, by comparing ΔG°of St-AcAHand Fe_3O_4@St-AcANCH, it can be found that kinetic of adsorption process for Fe_3O_4@St-AcANCH is quicker than that of St-AcAH.

Kinetic study

For practical applications, kinetics analysis of adsorption process during the design of an adsorption system is very important. For this purpose, pseudo-first-order and pseudo-second-order kinetic models (Eq. 6 and Eq. 7) were applied to investigate the kinetics parameters of heavy metal ions and dyes sorption onto both of bioadsorbents, and the most suitable model was applied for the experimental kinetic data. The kinetic parameters were calculated using equations listed in Table 4.

$$Pseudo\text{–}first\ order: \log(q_e - q_t) = log q_e - \frac{K_1 t}{2.303} \quad (6)$$

$$Pseudo\text{–}second\ order: \frac{t}{q_t} = \frac{1}{K_2 q_c^2} + \frac{t}{q_c} \quad (7)$$

where q_e and q_t are the equilibrium amounts of the metal ions adsorbed (mg g^{-1}) and contact time t (min), respectively. K_1 (1/min) is the rate constant for the first-order adsorption. K_2 (g/mg h) is the rate constant of second-order adsorption.

As shown in Table 4, the obtained values of the correlation coefficients (R^2) were closer to the unit via the pseudo-second-order kinetic model for both bioadsorbents. Accordingly, this model was better fitted with the kinetic data, also the rate of occupation of sites was found to be proportional to the square of the number of unoccupied sites on bioadsorbents.

Adsorption isotherm

Adsorption isotherms were utilized to explain the adsorption data by linear Langmuir and Freundlich isotherms. In these isotherms, the metal uptake per unit weight of the bioadsorbentq_e was related to the equilibrium concentration of adsorbate in the bulk fluid phase C_e. Purposing the design of sorption mechanism of heavy metal ions and dyes onto both of bioadsorbents, the adsorption isotherms were used. Two classical adsorption models, i.e., Langmuir and Freundlich isotherms were studied to find the best isotherm model that would well fit with the experimental results obtained from the considered system.

The Langmuir model describes saturated monolayer adsorption of solute molecules on a homogeneous site without any interaction between adsorbed ions. Unlike the Langmuir model, the Freundlich model describes the adsorption on heterogeneous surfaces with the interaction between adsorbed molecules [45]. The nonlinear form of Langmuir and Freundlich isotherms are shown in Eq. 8 and 9, respectively. According to the correlation coefficient (average of $R^2 = 0.99$ for both bioadsorbents) in Table 5, the adsorption of heavy metal ions and dyes on both of bioadsorbents fitted well to the Langmuir model via monolayer adsorption mechanism [46]. It can be also noted here that values of "n" as the degree of nonlinearity are larger than unit and indicating the physic-sorption process.

$$C_e/q_e = 1/(q_m b) + C_e/q_m \quad (8)$$

$$\log q_e = \log K_F + \left(1/n\right)\log C_e \quad (9)$$

C_e is the equilibrium concentration of Hg^{2+} metal ions in aqueous solution (mg L^{-1}), q_e and q_m are the equilibrium adsorption capacity and maximum adsorption capacity of the bioadsorbent (mg g^{-1}), respectively, and b is the Langmuir adsorption constant (L mg^{-1}). K_F and 1/n are Freundlich constants related to the sorption intensity and adsorption capacity, respectively. Comparing the prepared bioadsorbents of St-AcAH and Fe_3O_4@St-AcANCH with different bioadsorbents used for heavy metal ions and dyes removal in terms of adsorption capacity which indicated the remarkable capacity of the proposed bioadsorbents, especially Fe_3O_4@St-AcANCH [47–55].

Desorption and reusability

The reusability and recovery of heavy metal ions and dyes are important factors were done for evaluating the potential application of bioadsorbents. The preliminary results indicate that heavy metal ions or dyes loaded onto the samples can be easily desorbed with a single wash and using H_2SO_4 (0.1 M) or ethanol, respectively. St-AcAH and Fe_3O_4@St-AcANCH maintained nearly 66.0% and 89.1% of their original adsorption capacity after 7 consecutive cycles of adsorption-desorption, respectively. These results suggested the good performance and recyclability for both prepared bioadsorbents of heavy metal ions.

Conclusion

In short, St-AcAH and Fe_3O_4@St-AcANCH were synthesized through free radical copolymerization in aqueous solution. Incorporation of iron oxide nanoparticles onto the surface of St-AcAH was confirmed by multiple shifts in peak location of FTIR spectra of some functional groups such as

carboxylic or carboxylate. The presence of Fe_3O_4 nanoparticles in the Fe_3O_4@St-AcANCH was also shown using the results of the UV-visible and XRD, AFM, TGA analysis. TEM technique was also confirmed the presence of Fe_3O_4 with average particle size of 70 nm. The results indicated that the increasing of the amount of bioadsorbents resulted in an increase of Pb(II) and Cu(II) percentage removal, with a maximum of 93.83% and 99.32% CR and MV dyes with maximum adsorption of 96.7% and 97.5% for Fe_3O_4-St-AcANCH (0.2 g) respectively. However, the adsorption capacity of bioadsorbent was decreased at higher concentrations of 0.3–0.5 g. The highest removal efficiency for Cu(II) (95.4%), Pb(II) (88.4%), and MV (93.66%) is shown at pH 6.0, 5.5 and 7.4, respectively. On the other hand, the results indicated that kinetic of adsorption process for Fe_3O_4@St-AcANCH was quicker than that of St-AcAH and that was better fitted with the pseudo-second-order kinetic model**.** So, the rate of occupation of sites was found to be proportional to the square of the number of unoccupied sites on bioadsorbents. The reusability and recovery of heavy metal ions and dyes are important factors were also done for evaluating the potential application of bioadsorbents. St-AcAH and Fe_3O_4@St-AcANCH maintained nearly 66.0% and 89.1% of their original adsorption capacity after 7 consecutive cycles of adsorption-desorption, respectively. Taken together, these results strongly support the potential of Fe_3O_4-St -AcANCH for water treatment applications.

Acknowledgements The research leading to these results has received funding from the chemistry laboratory of Islamic Azad University, Tehran-North Branch.

References

1. Mauter MS, Zucker I, Perreault F, Werber JR, Kim JH, Elimelech M (2018). Nat Sustain 1(4):166
2. Yagub MT, Sen TK, Afroze S, Ang HM (2014). Adv Colloid Interf Sci 209:172–184
3. Gunatilake SK (2015) Methods 1(1):12
4. Tan KB, Vakili M, Horri BA, Poh PE, Abdullah AZ, Salamatinia B (2015). Sep Purif Technol 150:229–242
5. Ali I (2014). Sep Purif Rev 43(3):175–205
6. Li JJ, Wang CC, Hf F, Cui JR, Xu P, Guo J, Li JR (2017). Dalton Trans 46(31):10197–10201
7. Zhang L, Hu X, Wang C, Tai Y (2018). Mater Lett 231:80–83
8. Kim BC, Lee J, Um W, Kim J, Joo J, Lee JH, Kwak JH, Kim JH, Lee C, Lee H, Addleman RS (2011). J Hazard Mater 192(3):1140–1147
9. Zhang X, Wang Y, Chang X, Wang P, Pan B (2017). Environ Sci Nano 4(3):679–688
10. Sadiq MM, Li H, Hill AJ, Falcaro P, Hill MR, Suzuki K (2016). Chem Mater 28(17):6219–6226
11. Freitas T, Oliveira V, De Souza M, Geraldino H, Almeida V, Fávaro S, Garcia JC (2015). Ind Crop Prod 76:538–544
12. Mittal H, Ray SS, Okamoto M (2016). Macromol Mater Eng 301(5):496–522
13. Mittal H, Alhassan SM, Ray SS (2018). J Environ Chem Eng 6(6): 7119–7131
14. Yan H, Yang H, Li A, Cheng R (2016). Chem Eng J 284:1397–1405
15. Sharma G, Kumar A, Devi K, Sharma S, Naushad M, Ghfar AA, Ahamad T, Stadler FJ (2018). Int J Biol Macromol 114:295–305
16. Ruiz-Hitzky E, Darder M, Aranda P, Ariga K (2010). Adv Mater 22(3):323–336
17. Masuda F, Nishida K, Nakamura A (1978) Water absorbing starch resins. Google Patents
18. Akpalo E, Bidault L, Boissiere M, Vancaeyzeele C, Fichet O, Larreta-Garde V (2011). Acta Biomater 7(6):2418–2427
19. Qiu Y, Park K (2001). Adv Drug Deliv Rev 53(3):321–339
20. Byrne ME, Park K, Peppas NA (2002). Adv Drug Deliv Rev 54(1): 149–161
21. Thakur S, Sharma B, Verma A, Chaudhary J, Tamulevicius S, Thakur VK (2018). J Clean Prod 198:143–159
22. Sun W, Xue B, Li Y, Qin M, Wu J, Lu K, Wu J, Cao Y, Jiang Q, Wang W (2016). Adv Funct Mater 26(48):9044–9052
23. Sanchez C, Lebeau B, Ribot F, In M (2000). J Solgel Sci Technol 19:31–38
24. Sahraei R, Ghaemy M (2017). Carbohydr Polym 157:823–833
25. Ma Y, Lv L, Guo Y, Fu Y, Shao Q, Wu T, Guo S, Sun K, Guo X, Wujcik EK, Guo Z (2017). Polymer 128:12–23
26. Sharma G, Naushad M, Ala'a H, Kumar A, Khan MR, Kalia S, Bala M, Sharma A (2017). Int J Biol Macromol 95:484–493
27. Mallakpour S, Abdolmaleki A, Tabesh F (2018). Ultrason Sonochem 41:572–581
28. Peng N, Hu D, Zeng J, Li Y, Liang L, Chang C (2016). ACS Sustain Chem Eng 4(12):7217–7224
29. Hosseinzadeh H, Ramin S (2018). Int J Biol Macromol 106:101–115
30. Pour ZS, Ghaemy M (2015). RSC Adv 5(79):64106–64118
31. Dil NN, Sadeghi M (2018). J Hazard Mater 351:38–53
32. Kiatkamjornwong S, Thakeow P, Sonsuk M (2001). Polym Degrad Stab 73:363–375
33. Johnson DP (2001). Anal Chem 41:859–860
34. Alshehri SM, Aldalbahi A, Al-Hajji AB, Chaudhary AA, Panhuis N, Alhokbany N, Ahamad Y (2016). Carbohydr Polym 138:229–236
35. Zhu H, Zhu E, Ou G, Gao L, Chen J (2010). Nanoscale Res Lett 5(11):1755
36. Ghasemi E, Akbar Heydari A, Mika Sillanpää M (2017). Microchem J 131:51–56
37. Gutha Y, Zhang Y, Zhang W, Jiao W (2017). Int J Biol Macromol 97:85–98
38. Feng B, Hong R, Wang L, Guo L, Li H, Ding J, Zheng Y, Wei DG (2008). Colloids Surf A Physicochem Eng Asp 328:52–59
39. Cho DW, Jeon BH, Chon CM, Schwartz FW, Jeong Y, Song H (2015). J Inst Eng Chem 28:60–66
40. Saeedirad R, Ganjali ST, Bazmi M, Rashidi A (2018). J Taiwan Inst Chem Eng 82:10–22
41. Pacelli S, Paolicelli P, Pepi F, Garzoli S, Polini A, Tita B, Vitalone A, Casadei MA (2014). J Polym Res 21:409
42. Liu D, He L, Lei W, Klika KD, Kong L, Chen Y (2015). Adv Mater Interfaces 2:1500228
43. Wang J, Hao J, Liu D, Qin S, Chen C, Yang C, Liu Y, Yang T, Fan Y, Chen Y, Lei W (2017). Nanoscale 9:9787–9791
44. Ausavasukhi A, Kampoosaen C, Kengnok OJ (2015). Clean Prod 134:506–514
45. Crini G, Lichtfouse E, Wilson LD, Morin-Crini N (2019). Envirn Chem Lett 17:1–19
46. Lei W, Portehault D, Liu D, Qin S, Chen Y (2013) nature communications
47. Hosseinzadeh H, Khoshnood N (2016). Desalin Water Treat 57: 6372–6383

48. Panic VV, Velickovic SJ (2014). Sep Purif Technol 122:384–394
49. Ngwabebhoh AF, Erdem A, Yildiz UJ (2016). Appl Polym Sci 133: 43664
50. Mittal H, Maity A, Ray SS (2016). Appl Surf Sci 364:917–930
51. Oladipo AA, Gazi M, Yilmaz E (2015). Chem Eng Res Des 104: 264–279
52. Mohammed N, Grishkewich N, Berry RM, Tam KC (2015). Cellulose 22:3725–3738
53. Marandi GB, Kermani ZP, Kurdtabar M (2013). Polym-Plast Technol Eng 52:310–318
54. Mandal B, Ray SK (2013). Carbohydr Polym 98:257–269
55. Kumar N, Mittal H, Parashar V, Ray SS, Ngila (2016). JC RSC Adv 6:21929–21939